PHILOSOPHICAL TRANSACTIONS OF THE ROYAL SOCIETY A MATHEMATICAL PHYSICAL & ENGINEERING SCIENCES

The effect of edifice load on magma ascent beneath a volcano

Virginie Pinel

Phil. Trans. R. Soc. Lond. A 2000 **358**, 1515-1532
doi: 10.1098/rsta.2000.0601

THE ROYAL SOCIETY

The effect of edifice load on magma ascent beneath a volcano

By Virginie Pinel and Claude Jaupart

Laboratoire de Dynamique des Systèmes Géologiques, Institut de Physique du Globe de Paris, 4 Place Jussieu, 75252 Paris Cedex 05, France

A volcanic edifice exerts a large load at Earth's surface and modifies the stress field at depth. We investigate how this affects upward dyke propagation towards the surface. For given edifice dimensions and pressure conditions in the deep magma source, there is a critical density threshold above which magmas cannot reach the surface. This density threshold is a decreasing function of edifice height. For edifice heights in the range 0–3000 m, the density threshold spans the density range of common natural magmas (between 2700 and 2300 kg m^{-3}). With time, differentiation in a magma chamber generates increasingly evolved magmas with decreasing densities, which favours eruption. However, the edifice grows simultaneously at the surface, which counterbalances this effect. The general tendency is to gradually prevent more and more evolved magmas from reaching the surface. A volcanic edifice acts as a magma filter which prevents eruption and affects the chemical evolution of the chamber through its control on magma withdrawal. Thus, one may not consider that eruption products are random samples of an evolving magma reservoir. The partial destruction of an edifice may lead to renewed eruption of primitive and dense magmas.

Keywords: magma ascent; dyke propagation; edifice load

1. Introduction

A volcanic eruption is the end-result of a host of processes at depth, involving a largely unknown plumbing system and storage regions where magma crystallizes and differentiates. It is possible to document how magma evolves through petrological studies of erupted products. Over the lifetime of a volcano, lavas may not follow a complete magmatic differentiation series, showing that some magmas of intermediate composition do not get erupted. Such compositional gaps have been attributed to several mechanisms and in particular to the dynamics of magma chamber evolution. One must account for the eruption process because the chemical evolution of a reservoir depends on its volume budget, involving replenishment with primitive magmas and withdrawal of evolved magmas. There are failed eruptions, ending with the emplacement of 'cryptodomes' at shallow levels beneath the surface, which suggests that some magmas are expelled from the chamber but do not reach the surface. This is clearly the case at older volcanoes where erosion commonly exposes intrusive rocks, many of which did not feed surface eruptions. It is seldom feasible to determine the structure of a volcanic plumbing system, and hence fluid dynamical models have rarely been used for predicting whether or not magma of given composition

may be erupted. Similarly, there have been few attempts to predict how fast magma will travel from a storage region to the surface before the start of an eruption. Those are key questions for eruption forecasting.

Current geophysical techniques have poor spatial resolution, and hence the best constraints on the structure of volcanic systems come from the eruption record itself. Over long periods of time, a volcanic system changes with important implications for eruption behaviour. Two effects come into play. One is that magma composition changes due to storage and differentiation in a reservoir. This factor has been the subject of many investigations. The other factor has often been neglected and will be the main topic of this study. As a volcanic system develops over time, a volcanic edifice grows at the top. A volcano represents a large surface load, corresponding for example to 1 kbar for a 3000 m high edifice, which affects the local stress distribution at depth. Most models of volcanic eruptions say little about magma chambers and volcanic edifices, and pertain to eruptions out of open conduits. In initial stages of unrest, magma ascent is likely to proceed through fracturing, a mechanism which may be responsible for quite complex behaviour (Meriaux & Jaupart 1995). Here, we investigate the effect of a volcanic edifice on the stress field at depth and its implications for fracture propagation. We study how a volcanic edifice may prevent the eruption of some magmas. We conclude the paper with a short discussion of relevant volcanic phenomena.

2. Stress changes due to a volcanic edifice

(a) *Normal stress at the axis*

The volcanic edifice acts as a load applied at the Earth's surface. For simplicity, we consider an elastic half-space, which restricts our analysis to the upper crust. The elastic medium is characterized by Poisson's ratio, ν, and rigidity, G. We further simplify the problem by considering that the edifice is symmetric with respect to a vertical axis, which is a valid approximation for many continental strato-volcanoes. The elastic problem may be solved in cylindrical coordinates (r, θ, z) in which the two components of shear stress $\sigma_{r\theta}, \sigma_{\theta z}$, and the component of the displacement vector in the tangential direction u_θ, are zero everywhere. In this section, we choose z to be zero at the surface and to increase downwards.

The edifice can be characterized by three parameters: the maximum height h_v, its basal radius R and a shape factor. In order to evaluate the shape effect, we have considered two different edifice geometries: a circular slab of uniform thickness and a cone. The calculation method is outlined in Appendix A. Coordinates are scaled with radius R. In the following, unless specified otherwise, coordinates are dimensionless.

For a slab, the normal stress component σ_{rr} at the axis is given by

$$\frac{\sigma_{rr}}{\rho_\mathrm{m} g h_\mathrm{v}} = \frac{1}{2}\left[(1+2\nu) - \frac{2(1+\nu)z}{\sqrt{1+z^2}} + \frac{z^3}{(1+z^2)^{3/2}}\right], \tag{2.1}$$

where g is the acceleration due to gravity and ρ_m is the magma density. The vertical stress distribution is represented in figure 1. The maximum compression occurs at the base of the edifice. This stress changes sign at depth and becomes tensile. For $\nu = 0.25$, the maximum tension occurs at dimensionless depth $z = \sqrt{5}$ and is very small (less than 2% of the maximum compression). For a conical edifice, the stress

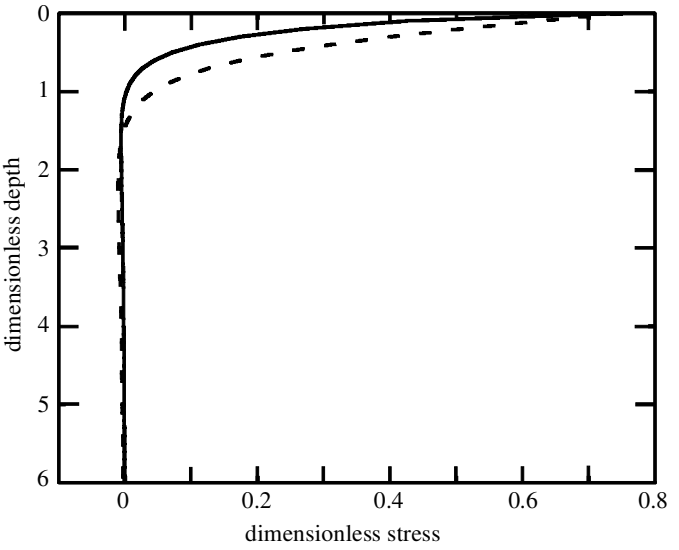

Figure 1. Normal stress σ_{rr} due to a volcanic edifice at the vertical axis as a function of depth. Stress and depth are scaled with $\rho_{\mathrm{m}} g h_{\mathrm{v}}$ and R, where h_{v} and R are the edifice height and radius, respectively. The dashed and full lines are for slab-shaped and conical edifices, respectively.

distribution may be obtained from the preceding result. The cone is built with slabs of infinitesimal thicknesses and a straightforward integration yields

$$\left.\begin{aligned} \frac{\sigma_{rr}}{\rho_{\mathrm{m}} g h_{\mathrm{v}}} &= \tfrac{1}{2}(1+2\nu) - (1+\nu) z \ln\left(\frac{1+\sqrt{1+z^2}}{z}\right) + \frac{1}{2}\frac{z}{\sqrt{1+z^2}}, && \text{for } z > 0, \\ \frac{\sigma_{rr}}{\rho_{\mathrm{m}} g h_{\mathrm{v}}} &= \tfrac{1}{2}(1+2\nu), && \text{for } z = 0. \end{aligned}\right\} \tag{2.2}$$

Figure 1 shows both stress distributions as a function of depth. At the base of the volcano, the axial normal stress does not depend on edifice shape. The normal stress decreases more rapidly with depth for a conical volcano than for a slab. Whatever the edifice shape, its effect is negligible at dimensionless depths larger than 3 (figure 1). This result can be used to evaluate the importance of conditions at large depths. We have taken an elastic half-space and hence the model is strictly valid only for lithospheres with elastic thicknesses larger than $3R$.

(*b*) *Stress distribution in a horizontal plane*

In Appendix A, we calculate the radial profiles of the two diagonal components of the in-plane components of the stress tensor, σ_{rr} and $\sigma_{\theta\theta}$ (figure 2). For $r/R < 0.2$, σ_{rr} varies by less that 5%. At $r = 0$, the radial component of displacement u_r is zero, which implies that $\sigma_{rr}(0, z) = \sigma_{\theta\theta}(0, z)$. We denote by $\sigma_{\mathrm{v}}(z)$ this common value. One may show that this equality remains approximately valid for small radial distances ($r/R < 0.2$). Thus, for conduits or fractures which are small compared with the edifice radius, one may assume a homogeneous stress field. The in-plane shear stress $\sigma_{r\theta}$ is zero everywhere. Thus, in the vicinity of the axis, the in-plane stress tensor

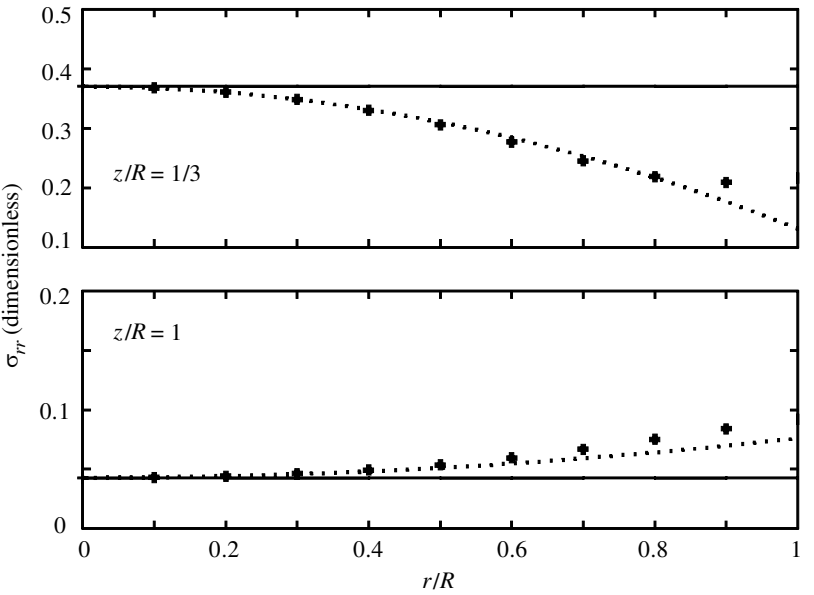

Figure 2. Normal stress σ_{rr} as a function of radial distance for two different depths below the surface and for a slab-shaped edifice. The dashed line shows the predictions of second-order expansions, and crosses correspond to the full solutions from equation (A 11) in Appendix A.

σ_H is such that

$$\begin{pmatrix} \sigma_{rr} & \sigma_{r\theta} \\ \sigma_{\theta r} & \sigma_{\theta\theta} \end{pmatrix} = \begin{pmatrix} \sigma_{\mathrm{v}} & 0 \\ 0 & \sigma_{\mathrm{v}} \end{pmatrix}. \tag{2.3}$$

Thus, the normal stress against any small vertical interface is equal to $\sigma_{\mathrm{v}}(z)$.

3. An equilibrium magma-filled fracture beneath an edifice

We consider that the unperturbed regional stress field is lithostatic in rocks of constant density ρ_{c}, corresponding to vertical pressure distribution $P_{\mathrm{l}}(z)$. Other regional stress fields can be treated using the same basic framework.

(a) *A critical density threshold for magmas*

Here, we look for static equilibrium of a vertical magma-filled fracture issuing from a reference level located at depth h (figure 3). This reference level is our starting point for stress calculations and may be either the top of a magma reservoir or some intermediate level in a longer fracture extending to greater depths. In the following, for the purposes of clarity, we take the z-axis to be oriented positively upwards, with $z = 0$ at the reference level. At this level, magma has developed overpressure ΔP_0 with respect to the surroundings. In this problem, the fracture width and length are very small compared with its height and one may consider deformation as purely horizontal. This is a common assumption in studies of fracture propagation (Lister 1990*a*, *b*; Valko & Economides 1995). The analysis above has shown that, at depth z, we may treat the fracture as if it were opening against a homogeneous pressure

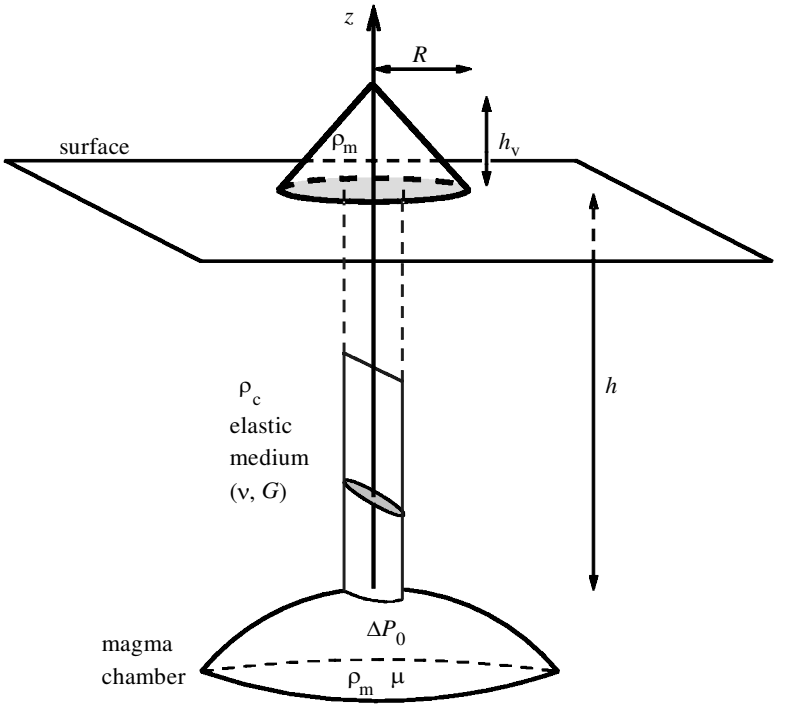

Figure 3. Diagram showing the basic set-up for the fluid dynamical model of magma ascent, with the main variables and parameters. Initial conditions are specified at some reference level, which may be either the top of a magma reservoir or some intermediate level in a longer fracture extending to greater depths.

field $P_l(z)+\sigma_v(z)$. In static conditions, this fissure is deformed by an internal magma overpressure, σ_{def}, which is due to the combined effects of the initial overpressure and magma buoyancy. At the fracture walls, the normal stress balance reads as follows,

$$P_l(z) + \sigma_v(z) + \sigma_{def}(z) = P_m(z), \tag{3.1}$$

where $P_m(z)$ is the magma pressure at height z. In static conditions,

$$P_m(z) = P_l(0) + \Delta P_0 - \rho_m g z, \tag{3.2}$$

and hence we obtain

$$\sigma_{def} = \Delta P_0 + (\rho_c - \rho_m) g z - \sigma_v. \tag{3.3}$$

Magma may reach the surface if and only if the fissure is held open for all z between 0 and h, that is to say if $\sigma_{def} > 0$. If this condition is not satisfied, i.e. if the stress due to the edifice is large enough to balance buoyancy and the initial overpressure, the static magma column cannot extend over the whole height h (figure 4). In such conditions, magma will be trapped at depth. For given initial level and edifice dimensions, one may rewrite this condition in terms of a lower bound on magma density. Magma may be erupted only if its density is less than the threshold value ρ_{crit} such

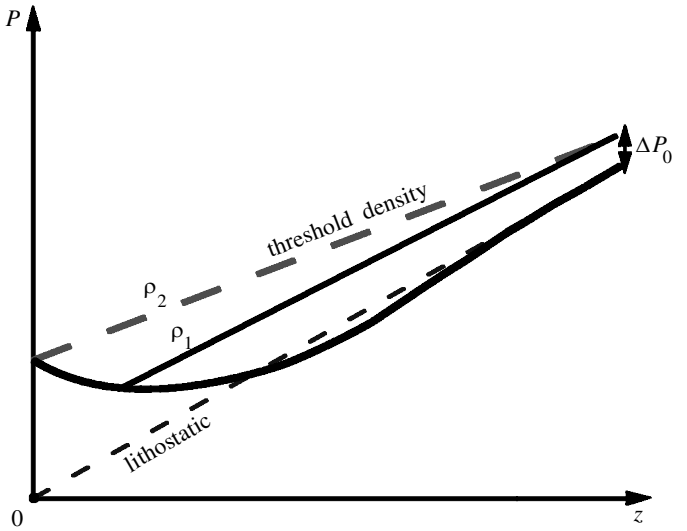

Figure 4. Schematic diagram showing vertical stress profiles beneath a volcanic edifice. The dashed line corresponds to the lithostatic stress field in the absence of the edifice and the thick continuous line shows the total stress profile when there is an edifice at the surface. Lines labelled ρ_1 and ρ_2 correspond to the pressure distributions within a vertical fracture extending from a magma chamber for two magma densities, such that $\rho_1 > \rho_2$. The maximum density for eruption is such that, at the base of the edifice, the fracture pressure is equal to the ambient stress.

that

$$\rho_{\mathrm{crit}} = 2\frac{\Delta P_0 + \rho_{\mathrm{c}} g h}{g(h_{\mathrm{v}}(1+2\nu)+2h)}. \tag{3.4}$$

This threshold density value is independent of edifice shape and radius, and its dependence on edifice height is shown in figure 5.

Taking an overpressure of 100 bar in a 10 km deep reservoir, a 500 m high volcano (which, for a 30° slope strato-volcano, corresponds to only 0.4 km^3 of erupted products) will cause a compressive stress large enough to prevent the densest magmas (typically basalts) from reaching the surface. A higher volcanic edifice prevents the ascent of lighter magmas. Magma densities have values in the 2300–2700 $\mathrm{kg\,m}^{-3}$ range, and a usual trend is for magma density to decrease with the degree of differentiation. As shown by figure 5, edifice heights which are common on Earth are able to stop the ascent of many natural magmas.

(*b*) *Discussion*

We have only considered dry melt, whereas most natural magmas contain significant amounts of volatiles. Gas exsolution during ascent leads to a density decrease for the rising mixture and hence to a buoyancy increase. Thus, with magmatic gases added, the ability of a magma to reach the surface is enhanced, and the threshold density is higher. We have calculated the critical density for different gas contents in Appendix B, and find that a volcanic edifice remains able to prevent many natural magmas from erupting (figure 6).

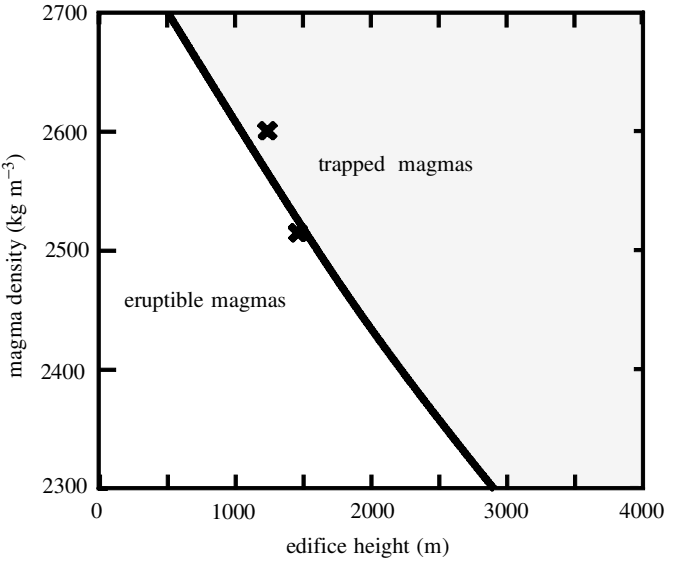

Figure 5. Critical magma density threshold as a function of edifice height. The critical density depends on several variables, ΔP_0, h, ρ_c and ν (equation (3.4)), whose values are given in table 1. The line separates two domains: to the left, magma can reach the surface and erupt, to the right, magma gets trapped beneath the surface. The two crosses indicate the set of conditions used in dynamical calculations of dyke propagation (table 1).

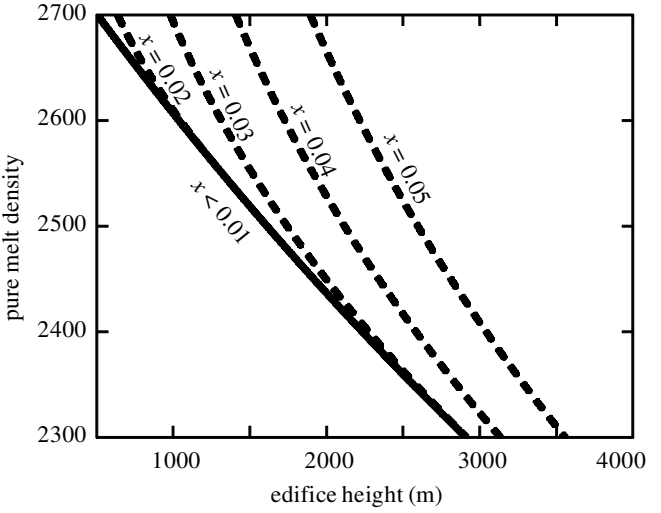

Figure 6. Critical density as a function of edifice height for different dissolved water contents. Numbers along the curves are values of water concentration. The calculation method is explained in Appendix B.

According to this model, when eruptions are fed from a magma reservoir, the ability of an edifice to behave as a density filter throughout the lifetime of the volcanic system depends on the depth and size of the reservoir. The depth of the reservoir determines the magnitude of the total buoyancy force available. The size of the

reservoir affects the time-variation of the different parameters (ΔP_0, h_v, ρ_m) because it acts on the amount of magma available to build the volcano and influences the rate of magmatic differentiation.

4. Fracture propagation beneath a volcano

We now evaluate the effect of the volcanic edifice on magma transport. We consider a magma-filled fracture which rises towards Earth's surface. As shown by many authors, we may neglect the strength of the surrounding rocks in the force balance for dyke propagation, and hence do not treat stress singularity at the tip (Lister 1990*a*, *b*). We focus on the interplay between buoyancy, viscous effects and elastic stresses. For the sake of simplicity, we consider a fracture of given length $l = 2a$, which is being opened due to magma pressure. This fissure is opened providing the deformation stress σ_def is positive. We rewrite the normal stress balance at the fracture walls with the added effect of flow-induced stresses. The deformation stress is now given by

$$\sigma_\mathrm{def} = \Delta P_0 + (\rho_\mathrm{c} - \rho_\mathrm{m})gz - \sigma_\mathrm{v} + p, \tag{4.1}$$

where p is the head loss due to flow in the propagating fracture. Under this applied stress, the fracture opens and adopts an elliptical cross-section with semi-axes a and b. In this case, σ_def is equal to (Mushkhelishvili 1963)

$$\sigma_\mathrm{def}(z,t) = \frac{G}{1-\nu} b(z,t) \left[a + \frac{(1-2\nu)b(z,t)}{2(1-\nu)} \right]^{-1}. \tag{4.2}$$

In this problem, $b(z,t) \ll a$, and hence

$$\sigma_\mathrm{def}(z,t) \approx \frac{G}{1-\nu} \frac{b(z,t)}{a}. \tag{4.3}$$

The magma is considered as a Newtonian, viscous and incompressible fluid. For typical volcanic conditions, flow proceeds in a laminar regime. The open fracture has an elliptical cross-section and the momentum equation may be integrated in the horizontal plane at each height z to solve for the local volumetric flux rate (White 1991):

$$q(z,t) = -\frac{\pi}{4\mu} \frac{a^3 b^3}{a^2 + b^2} \frac{\partial p(z,t)}{\partial z}, \tag{4.4}$$

where μ is the magma viscosity. Using again the fact that $b(z,t) \ll a$, this may be simplified as follows:

$$q(z,t) = -\frac{\pi}{4\mu} \frac{\partial p(z,t)}{\partial z} a b^3. \tag{4.5}$$

Applying the equation of continuity, we obtain

$$\frac{\partial \pi a b(z,t)}{\partial t} = -\frac{\partial q(z,t)}{\partial z}. \tag{4.6}$$

Using equations (4.1), (4.3), (4.5) and (4.6), the fracture width b is the solution of the following equation:

$$\frac{\partial b(z,t)}{\partial t} = -\frac{(\rho_c - \rho_m)g}{4\mu}\frac{\partial b^3}{\partial z} + \frac{G}{16\mu a(1-\nu)}\frac{\partial^2 b^4}{\partial z^2} + \frac{1}{4\mu}\frac{\partial}{\partial z}\left(\frac{\mathrm{d}\sigma_v}{\mathrm{d}z}b^3\right). \tag{4.7}$$

We present calculations for a conical edifice, such that σ_v is given by equation (2.2). Calculations with a slab do not lead to significant differences, which shows that the shape of the edifice plays a minor role. We scale pressures by the chamber overpressure, ΔP_0, and depth z by the reservoir depth h. We obtain the following scales for time, flux and fissure width:

$$[t] = \frac{16\mu h^2 G^2}{\Delta P_0^3 a^2 (1-\nu)^2}, \tag{4.8}$$

$$[Q] = \frac{(1-\nu)^4 \Delta P_0^5 a^4}{16 G^4 \mu h}, \tag{4.9}$$

$$[b] = \frac{\Delta P_0 a(1-\nu)}{G}. \tag{4.10}$$

The time-scale $[t]$ is for opening the fissure over length h with a uniform overpressure equal to ΔP_0. In reality, pressures are everywhere smaller than this, and hence this time-scale provides an upper bound for the rise time over height h. The length-scale $[b]$ is the fracture width due to an overpressure ΔP_0. Three dimensionless numbers appear. $R_1 = (\rho_m - \rho_c)gh/\Delta P_0$ and $R_2 = (\rho_m g h_v)/\Delta P_0$ characterize the magnitudes of buoyancy force and edifice stress scaled to the initial overpressure. Clearly, the key factors are the relative magnitudes of the driving pressure terms and the edifice-induced stress. The dimensionless number $R_3 = R/h$ provides a measure of the extent of the zone affected by the edifice stress. The dimensionless problem to solve is

$$\begin{aligned}
\frac{\partial b(z,t)}{\partial t} &= 4R_1\frac{\partial b^3}{\partial z} + \frac{\partial^2 b^4}{\partial z^2} + 4\frac{\partial}{\partial z}\left(\frac{\mathrm{d}\sigma_v}{\mathrm{d}z}b^3\right),\\
\sigma_v(z) &= R_2\left[\tfrac{1}{2}(1+2\nu) + \frac{(1-z)}{2\sqrt{R_3^2+(1-z)^2}}\right]\\
&\quad - \frac{R_2}{R_3}(1+\nu)(1-z)\ln\left(\frac{R_3+\sqrt{R_3^2+(1-z)^2}}{1-z}\right),\\
b_{(z=0,t)} &= 1 - \sigma_{v(z=0)}.
\end{aligned} \tag{4.11}$$

This problem was solved numerically with a semi-implicit finite difference scheme with Dirichlet boundary conditions. The fracture half-width $b(0)$ at the reference level is fixed by the initial overpressure. Convergence was verified by comparing runs with different space- and time-steps. We checked that mass conservation was satisfied on the scale of the whole dyke, which requires the instantaneous volume change to be equal to the basal flux.

We first discuss results obtained for the case of magma with a density slightly smaller than the threshold density. The parameters used are given in table 1. The calculations were stopped when the dyke was 100 m from the surface. We choose not to carry out calculations within the edifice itself because it may not behave as an elastic solid. However, the same basic physical principles apply. Figure 7 shows how

Table 1. *Parameters and physical properties used in the calculations*

Geometrical parameters (m)		
depth of the reservoir	h	10 000
edifice radius	R	3000
edifice height	h_v	1500 (case 1) or 1200 (case 2)
half-length of the fracture	a	100
Physical properties		
Poisson's ratio	ν	0.25
rigidity (Pa)	G	1.125×10^9
density of surrounding rocks (kg m^{-3})	ρ_c	2700
density of magma (kg m^{-3})	ρ_m	2510 (case 1) or 2600 (case 2)
initial overpressure (Pa)	ΔP_0	10^7
viscosity (Pa s)	μ	10^5
Scale		
time-scale (s)	$[t]$	$3.6\,10^7$
flux scale (m^3 s^{-1})	$[Q]$	1.23×10^{-4}
fissure width scale (m)	$[b]$	0.67

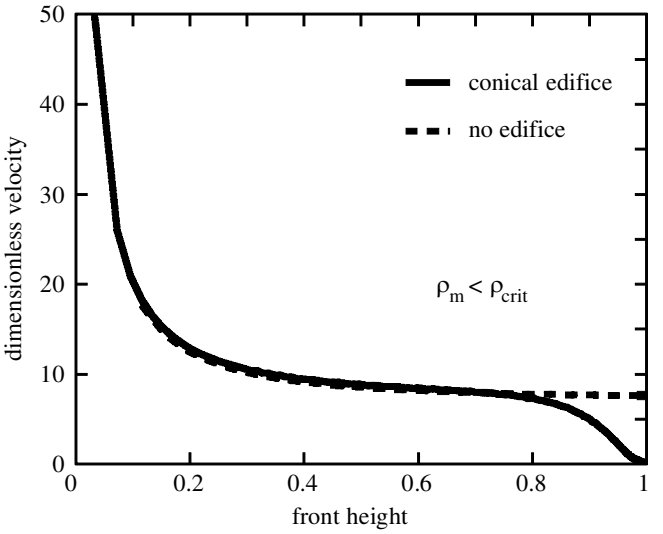

Figure 7. Dimensionless fracture tip velocity as a function of height above the reference level for magma density smaller than the threshold value. Parameters for these calculations correspond to case 1 in table 1.

the propagation rate evolves as the fracture rises. At great depth, the presence of an edifice tends to enhance the propagation rate because it generates tension, but this is a small effect. When the dyke reaches a depth close to the volcano radius R, the propagation rate drops markedly. Just before the dyke reaches the surface, this rate is 100 times smaller than the initial value. Figure 8 shows how the dyke shape

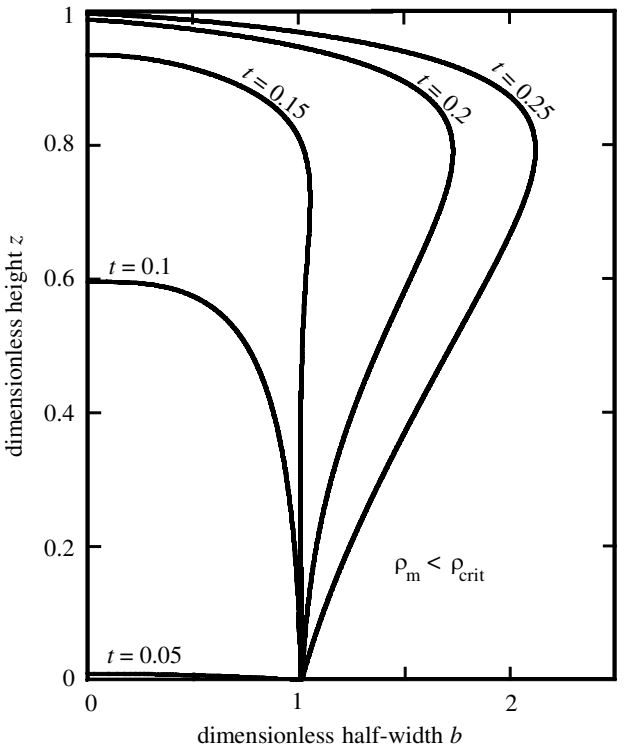

Figure 8. Dimensionless fracture width as a function of height at different times for magma density smaller than the threshold value. Note the inflated nose region which develops when the fracture tip is at shallow depth beneath the edifice. Parameters for these calculations correspond to case 1 in table 1.

evolves with time. As the propagation rate decreases, the total dyke volume keeps on increasing, mostly due to deformation near the dyke tip. As the dyke gets close to the surface, the supply rate diminishes markedly and the dyke volume increases at a reduced rate (figure 9).

For magma densities above the threshold value, magma is too dense to reach the surface and we find that the flow rate decreases until a state of equilibrium is achieved (figure 10). The propagation rate drops to very small values as the fracture tip gets close to the equilibrium height given by the static calculations developed above. At such late stages of dyke ascent, however, magma is still flowing into the open fracture and the volume of stored magma stored keeps on increasing (figure 11). The new magma ponds at the tip of the fracture, which develops a permanent inflated nose reminiscent of cryptodome structures (figure 12). In this situation, a significant volume of magma may get stored beneath the surface.

5. Implications for eruption behaviour

A detailed comparison of the predictions of our model to natural volcanoes is outside the scope of this paper, and we restrict ourselves to a few salient observations. Our aim is to evaluate how one may reconsider the field evidence in the light of the simple physical principles shown above.

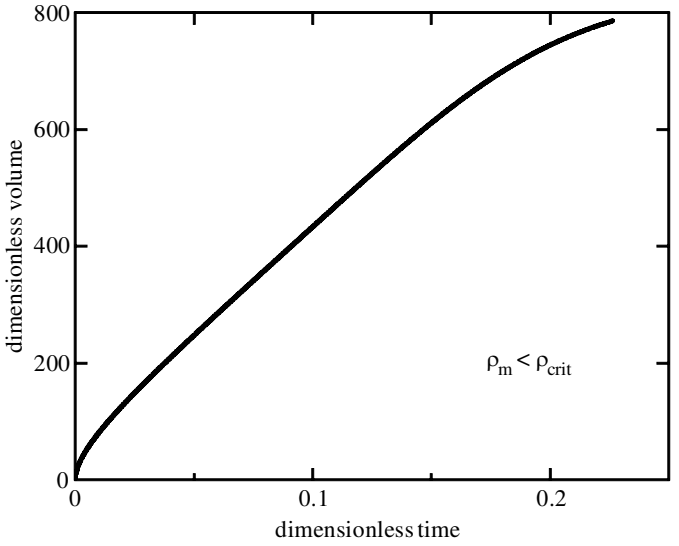

Figure 9. Dimensionless magma volume within the fracture as a function of time for magma density smaller than the threshold value. Parameters for these calculations correspond to case 1 in table 1. Note that the rate of volume increase slows down markedly when the fracture tip is at shallow depth beneath the edifice.

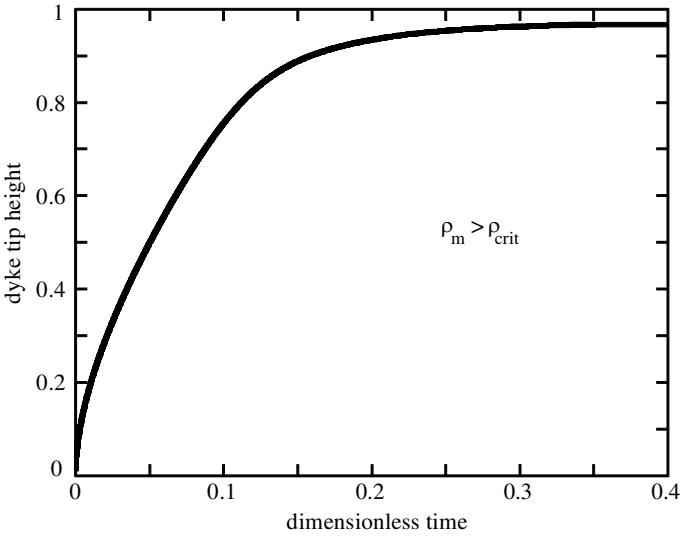

Figure 10. Dimensionless tip height as a function of dimensionless time for magma density larger than the threshold value. Parameters for these calculations correspond to case 2 in table 1.

(*a*) *Mt St Helens 1980*

The chronology of events preceding the 18 May 1980 eruption of Mt St Helens supports the inferences drawn from the theory. Magma was issued from a deep reservoir located at a depth of approximately 8 km (Rutherford & Hill 1993). The first sign of unrest was an increase of local seismicity levels on March 15 (Endo *et al.* 1981). On

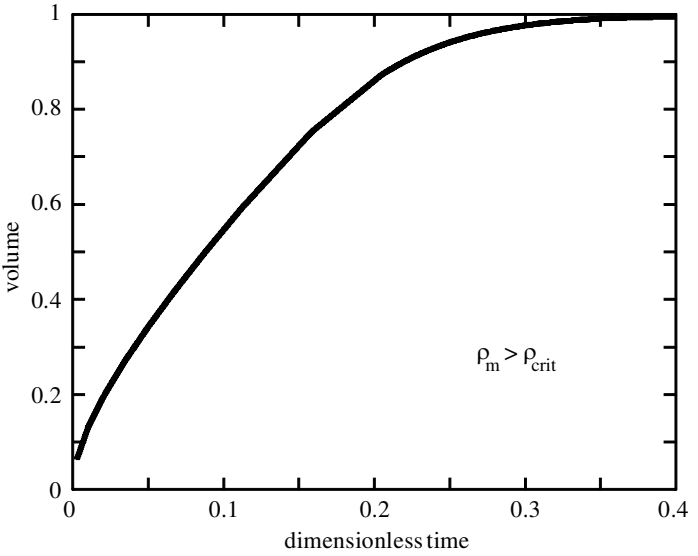

Figure 11. Magma volume within the fracture as a function of dimensionless time for magma density larger than the threshold value. The magma volume is shown as the fraction of the final value achieved when mechanical equilibrium conditions are established. The volume of stored magma keeps on increasing for times larger than 0.2, even though the fracture tip has stopped rising (see figure 10). Parameters for these calculations correspond to case 2 in table 1.

20 March seismic events showed that magma was already 4 km beneath the surface. March 27 marked the onset of phreatic activity and a bulge started to grow on the edifice flank. From the dimensions of the bulge and the distribution of seismicity, magma was probably no more than 1 km below the surface (Moore & Albee 1981). It then took more than 20 days for the eruption proper. This sequence of events clearly indicates that the ascent rate decreased with time, as magma was getting closer and closer to the surface. Magma took a few days to rise over 5 or 6 km, an extra week for the next 3 or 4 km, and then three weeks for the last kilometre or so. A fracture rising through an elastic medium in lithostatic equilibrium (i.e. with no edifice) would not exhibit such behaviour. The decreasing rates of upward propagation and cryptodome growth, as well as the apparent stalling of the magma near the surface, are consistent with our results (figure 7). The eruption was triggered by flank failure and may not have happened if the flank had held fast.

At Mt St Helens, field evidence suggests that the fracture had almost stopped rising in early May. Petrological and isotopic data also indicate magma arrest at shallow levels (Hoblitt & Harmon 1993; Cashman & Blundy, this issue). Interestingly, there is also evidence for temporary magma storage at small depths beneath the surface during the 1991 eruption of Mt Pinatubo (Cashman & Blundy, this issue).

(*b*) *The volcanic edifice as an evolving density filter*

At Mount Mazama, Oregon, the various erupted magmas are not distributed in a random fashion. The edifice is made of intermediate to evolved lavas, dacite, andesite and rhyodacite. Primitive magmas were available throughout the volcano history, as shown by the rather abundant flows of olivine-bearing basalt or mafic andesite

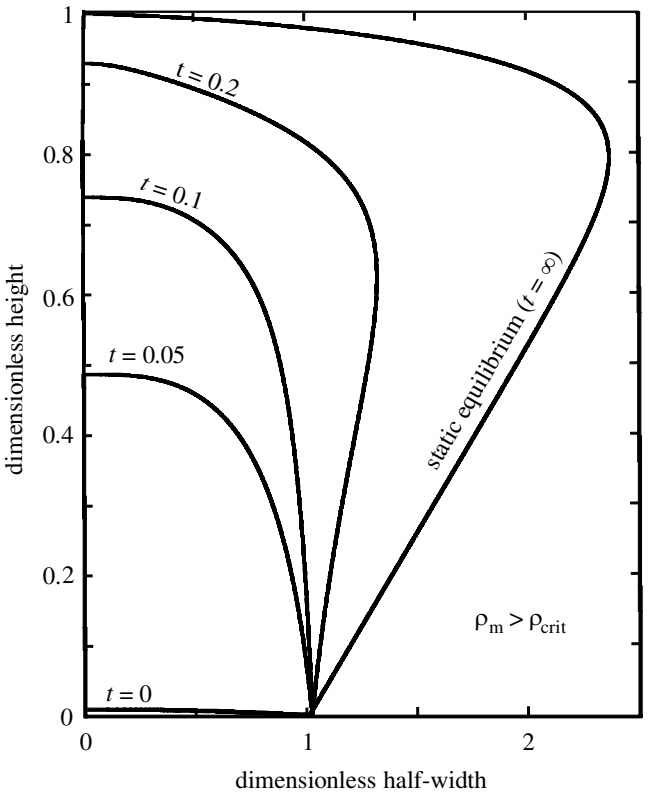

Figure 12. Dimensionless fracture width as a function of height at different times for magma density larger than the threshold value. Parameters for these calculations correspond to case 2 in table 1.

found a few kilometres from the caldera (Bacon 1983). These magmas have the same compositions as the parent magmas for the differentiated products, but they have not been erupted through the focal region (Bacon & Druitt 1988). This has been called the 'shadow zone' effect (Bacon 1985). One explanation for this is that the mafic magmas cannot go through the shallow magmatic reservoir beneath the edifice (Bacon 1985). However, this does not explain why there was a reservoir at this particular location and not elsewhere, where many mafic intrusions are documented. We suggest that, in fact, the reservoir grew because an edifice was being built at the surface.

Another interesting case is provided by Mount Adams, southern Washington. This volcano shows the same basic features as Mount Mazama, with andesitic–dacitic lavas in the focal region and dominantly basaltic lavas at the periphery, more than 5 km from the summit. Differentiation was achieved in small magma batches (Hildreth & Lanphere 1994), which indicates that there was never a large reservoir beneath the volcano. Thus, in this case, it is difficult to rely on the shadow zone effect. Further clues are that, at Mount Adams, between 940 and 520 ka, 80% of the products are basaltic, and that the proportion of andesite only starts increasing with the first cone-building episode (Hildreth & Lanphere 1994).

(*c*) *Destruction of the volcanic edifice*

The filter effect of the volcanic edifice can be illustrated in reverse when the height of the edifice gets reduced through landslides or large explosive eruptions. One expects a close temporal association between such events and a return to more primitive, and hence denser, lavas. At Mount Mazama, the 7000 yr BP climactic eruption destroyed the edifice. This volcano had only erupted rhyodacite lavas for several thousand years before this catastrophe, and started to erupt mafic andesite afterwards (Bacon 1983). At Mt St Helens, the Pine Creek period (3000–2500 yr BP) ended with large landslides due to massive slope failure (Hausback & Swanson 1990). This eruptive period involved dacitic lavas exclusively and was followed by the onset of andesitic and basaltic volcanism in the Castle Creek period.

6. Conclusion

Our calculations show that a volcanic edifice acts to prevent dense magmas from reaching the surface. Furthermore, as the edifice grows, the critical density changes, and hence so do the magma compositions which may not get erupted. The key point is that edifice growth and magmatic differentiation work in parallel. As crystallization and differentiation proceed, the residual magma usually tends to become less dense, which favours eruption. However, at the same time, the edifice grows, which counteracts the effect of the chemical change. One may not consider that an evolving magma reservoir gets sampled randomly by eruptions. The edifice acts as a regulating valve, which sets magmatic differentiation on a specific course.

Appendix A. Stresses due to a volcanic edifice

We consider a slab of thickness h_v and radius R at the Earth's surface. z is the vertical coordinate, oriented positively downwards. At $z = 0$, boundary conditions are as follows:

$$\begin{aligned} \sigma_{zz(z=0,r)} &= \rho_\mathrm{m} g h_\mathrm{v} \qquad \text{for } r \leqslant R, \\ &= 0 \qquad\qquad \text{for } r > R, \end{aligned} \tag{A 1}$$

$$\sigma_{rz(z=0,r)} = 0, \tag{A 2}$$

$$\sigma_{ij} \text{ finite as } z \text{ tends to infinity}, \tag{A 3}$$

where ρ_m is the average density of material in the edifice. Our sign convention is such that a compression corresponds to a positive stress. In cylindrical coordinates, we use the method outlined by Sneddon (1951). The scalar function Φ is such that

$$u_r = -\frac{\lambda+\mu}{\mu}\frac{\partial^2 \Phi}{\partial r \partial z}, \tag{A 4}$$

$$u_z = \frac{\lambda+2\mu}{\mu}\nabla^2 \Phi - \frac{\lambda+\mu}{\mu}\frac{\partial^2 \Phi}{\partial z^2}. \tag{A 5}$$

Φ is a solution of the biharmonic equation,

$$\nabla^4 \Phi = 0, \tag{A 6}$$

with the relevant boundary conditions. Introducing the zero-order Hankel transform,

$$G(\xi, z) = \int_0^\infty r\Phi(r, z) J_0(\xi r)\, \mathrm{d}\xi, \tag{A 7}$$

the biharmonic equation becomes

$$\left(\frac{\partial^2}{\partial z^2} - \xi^2\right)^2 G(\xi, z) = 0, \tag{A 8}$$

which has the following solution:

$$G(\xi, z) = (A + Bz)\mathrm{e}^{-\xi z}. \tag{A 9}$$

The constants A and B are found through the boundary conditions on σ_{rz} and σ_{zz}:

$$G(\xi, z) = \frac{\rho_\mathrm{m} g h_\mathrm{v} R}{2\xi^3(\lambda + \mu)} J_1(R\xi)\left(\frac{\lambda}{(\lambda + \mu)\xi} + z\right)\mathrm{e}^{-z\xi}. \tag{A 10}$$

Using (A 10) and Hooke's law, σ_{rr} is given by

$$\sigma_{rr} = \int_0^\infty f(\xi, z) J_0(\xi r)\, \mathrm{d}\xi + \int_0^\infty g(\xi, z)\frac{J_1(\xi r)}{r}\, \mathrm{d}\xi \tag{A 11}$$

where

$$f(\xi, z) = \rho_\mathrm{m} g h_\mathrm{v} R J_1(\xi l)\mathrm{e}^{-\xi z}(1 - \xi z), \tag{A 12}$$

$$g(\xi, z) = \rho_\mathrm{m} g h_\mathrm{v} R J_1(\xi l)\mathrm{e}^{-\xi z}\left(z - \frac{\mu}{\xi(\lambda + \mu)}\right). \tag{A 13}$$

These expressions have been used to calculate stresses everywhere. We are interested in stresses near the axis, for small r, and hence expand the above equation for $r \approx 0$:

$$\sigma_{rr}(r, z) = \sigma_{rr}(0, z) + r\left(\frac{\partial \sigma_{rr}}{\partial r}\right)_{r=0} + \frac{r^2}{2}\left(\frac{\partial^2 \sigma_{rr}}{\partial r^2}\right)_{r=0} + \cdots, \tag{A 14}$$

which leads to

$$\begin{aligned}\sigma_{rr}(r, z) = &\int_0^\infty f(\xi, z)(J_0(0) + r\xi \dot{J}_0(0) + \tfrac{1}{2} r^2 \xi^2 \ddot{J}_0(0))\, \mathrm{d}\xi \\ &+ \int_0^\infty g(\xi, z)\xi\left(\lim_{r\to 0}\frac{J_1(\xi r)}{\xi r} + r\xi \lim_{r\to 0}\frac{\partial J_1/\xi r}{\partial \xi r} + \frac{r^2\xi^2}{2}\lim_{r\to 0}\frac{\partial^2 J_1/\xi r}{\partial(\xi r)^2}\right)\mathrm{d}\xi + \cdots.\end{aligned} \tag{A 15}$$

We use the polynomial expansions of the various Bessel functions:

$$\left.\begin{aligned} J_0(0) &= 1, & \lim_{x\to 0}\frac{J_1(x)}{x} &= 0.5, \\ \dot{J}_0(0) &= 0, & \lim_{x\to 0}\frac{\partial J_1(x)/x}{\partial x} &= 0, \\ \ddot{J}_0(0) &= -2\frac{2.24\ldots}{9}, & \lim_{x\to 0}\frac{\partial^2 J_1(x)/x}{\partial x^2} &= -2\frac{0.56\ldots}{9}. \end{aligned}\right\} \tag{A 16}$$

Terms of order 1 are thus zero, which was expected as the stress has an extremum at the axis. To extend the expansion to second order, we use the following result:

$$\int_0^\infty \mathrm{e}^{-\xi z} J_1(R\xi) = \frac{1}{R} - \frac{z}{R\sqrt{R^2+z^2}} \tag{A 17}$$

and its derivatives with respect to z. Using dimensionless variables, as in the main text, we find that, at zero order, the two diagonal stress components are identical:

$$\sigma^0_{rr}(z) = \sigma^0_{\theta\theta}(z) = \frac{1}{2}\left[(1+2\nu) - \frac{2(1+\nu)z}{\sqrt{1+z^2}} + \frac{z^3}{(1+z^2)^{3/2}}\right]. \tag{A 18}$$

Second-order expansions are slightly different:

$$\sigma_{rr}(z) = \sigma^0_{rr}(z) + \frac{z}{3}\left[\frac{0.56(1-2\nu) - 2.24}{(1+z^2)^{5/2}} + \frac{(2.24-0.56)(4z^2-1)}{(1+z^2)^{7/2}}\right] r^2 + \cdots, \tag{A 19}$$

$$\sigma_{\theta\theta}(z) = \sigma^0_{\theta\theta}(z) + \frac{z}{3}\left[\frac{-0.56(1-2\nu) - 2.24*4\nu}{(1+z^2)^{5/2}} + \frac{0.56(4z^2-1)}{(1+z^2)^{7/2}}\right] r^2 + \cdots. \tag{A 20}$$

These results emphasize that the stresses vary by negligible amounts for small r. In practice, there are no significant variations for $r \leqslant 0.2$. Figure 2 compares the full values with predictions from the second-order expansion, and it may be seen that they agree very well up to $r \approx 0.5$.

Appendix B. Gas phase in a static magma column

The pressure inside a static magma-filled fracture obeys the hydrostatic equation:

$$\frac{\mathrm{d}P}{\mathrm{d}z} = -\rho_\mathrm{m} g. \tag{B 1}$$

If the gas phase is present with mass fraction x_g, the vesicular magma density is

$$\frac{1}{\rho_\mathrm{m}} = \frac{x_g}{\rho_g} + \frac{1-x_g}{\rho_\mathrm{mo}}, \tag{B 2}$$

where ρ_g and ρ_mo are the densities of gas and melt phases, respectively. For magma with given volatile concentration x_i, corresponding to saturation pressure P_s, the mass fraction of gas at pressure P less than P_s is given by

$$x_g \approx x(P_\mathrm{s}) - x(P). \tag{B 3}$$

We use the ideal gas law, which is appropriate for crustal conditions,

$$\rho_g = \frac{MP}{RT}, \tag{B 4}$$

with M the molar mass and R the perfect gas constant. Finally, we take the usual empirical solubility law,

$$x = sP^n, \tag{B 5}$$

with $s = 4.11 \times 10^{-6}$ and $n = 0.5$.

For given x_i, we integrate the pressure equation up the magma column and obtain the vertical profiles of gas content and density. The gas phase acts to decrease the density of magma with respect to the pure melt phase, and hence to enhance buoyancy. We calculate the threshold melt density value as a function of edifice height, as in the main text. Figure 6 shows sample calculations for $h = 10^4$ m, $\Delta P_0 = 10^7$, $\rho_c = 2700$ kg m^{-3} and various values of x_i. An initial water concentration of 1 wt% is too small to affect the results significantly. With increasing water content, for a given edifice height, the threshold melt density increases. However, one may see that the critical density remains within the range of natural magmas, which demonstrates that the 'filter' effect of the edifice still operates.

We thank Stephen Sparks and Jurgen Neuberg for stimulating discussions and comments, and referees for their suggestions. Support for this study was provided by INSU/CNRS (PNRN programme).

References

Bacon, C. R. 1983 Eruptive history of Mount Mazama and Crater Lake caldera, Cascade Range, U.S.A. *J. Volcanol. Geotherm. Res.* **18**, 57–115.

Bacon, C. R. 1985 Implications of silicic vent patterns for the presence of large crustal magma chambers. *J. Geophys. Res.* **90**, 11 243–11 252.

Bacon, C. R. & Druitt, T. H. 1988 Compositional evolution of the zoned calcalkaline magma chamber of Mount Mazama, Crater Lake, Oregon. *Contrib. Mineral. Petrol.* **98**, 224–256.

Endo, E. T., Malone, S. D., Noson, L. L. & Weaver, C. S. 1981 Locations, magnitudes, and statistics of the March 20–May 18 earthquake sequence. In *The 1980 eruptions of Mount St. Helens, Washington* (ed. P. W. Lipman & D. R. Mullineaux), pp. 93–107. US Geological Survey Professional Paper 1250.

Hausback, B. P. & Swanson, D. A. 1990 Record of prehistoric debris avalanches on the North flank of Mount St. Helens Volcano, Washington. *Geoscience Canada* **17**, 142–145.

Hildreth, W. & Lanphere, M. A. 1994 Potassium–argon geochronology of a basalt–andesite–dacite arc system: the Mount Adams volcanic field, Cascade Range of southern Washington. *Geol. Soc. Am. Bull.* **106**, 1413–1429.

Hoblitt, R. P. & Harmon, R. S. 1993 Bimodal density distribution of cryptodome dacite from the 1980 eruption of Mount St. Helens, Washington. *Bull. Volcanol.* **55**, 421–437.

Lister, J. R. 1990*a* Buoyancy-driven fluid fracture: the effects of material toughness and low-viscosity precursors. *J. Fluid Mech.* **210**, 263–280.

Lister, J. R. 1990*b* Buoyancy-driven fluid fracture: similarity solutions for the horizontal and vertical propagation of fluid-filled cracks. *J. Fluid Mech.* **217**, 213–239.

Meriaux, C. & Jaupart, C. 1995 Simple fluid dynamic models of volcanic rift zones. *Earth Planet. Sci. Lett.* **136**, 223–240.

Moore, J. G. & Albee, W. C. 1981 Topographic and structural changes, March–July 1980—photogrammetric data. In *The 1980 eruptions of Mount St. Helens, Washington* (ed. P. W. Lipman & D. R. Mullineaux), pp. 123–134. US Geological Survey Professional Paper 1250.

Mushkhelishvili, N. I. 1963 *Some basic problems in the mathematical theory of elasticity.* The Netherlands: Noordhoff.

Rutherford, M. J. & Hill, P. M. 1993 Magma ascent rates from amphibole breakdown: an experimental study applied to the 1980–1986 Mount St. Helens eruptions. *J. Geophys. Res.* **98**, 19 667–19 685.

Sneddon, I. N. 1951 *Fourier transforms.* McGraw-Hill.

Valko, P. & Economides, M. J. 1995 *Hydraulic fracture mechanics.* Wiley.

White, F. M. 1991 *Viscous fluid flow*, 2nd edn. McGraw-Hill.